Sub-stoichiometric functionally graded titania fibres for water-splitting applications

Vaia Adamaki[1], A. Sergejevs[2], C.Clarke[2], F. Clemens[3], F. Marken[4], C.R.Bowen[1]

[1]*Mechanical Engineering Department, University of Bath, Bath, UK*
Email: v.adamaki@bath.ac.uk, web site: http://people.bath.ac.uk/va253/index.html

[2]*Electronic and Electrical Engineering Department, University of Bath, Bath, UK*

[3]*High Performance Ceramics, EMPA Materials Science and Technology, Zurich, Switzerland*
[4]*Chemistry Department, University of Bath, Bath, UK*

Abstract

The photo-electro-chemical (PEC) splitting of water requires semiconductor materials with a minimum energy gap of 1.23eV along with conduction and valence bands overlapping the oxidation of H_2O and reduction of H^+ respectively. The aim of this work is to overcome the limitations of stoichiometric titania by manufacturing fine scale fibres that exhibit a compositional gradient of oxygen vacancies across the fibre length. In such a configuration the fibre end that is chemically reduced to a relatively small extent acts as the photoanode and the oxygen vacancies enhance the absorption of light. The fibre end that is reduced the most consists of Magnéli phases and exhibits metallic electrical conductivity that enhances the electron-hole separation. The structure and composition of the functionally graded fibres that were manufactured through extrusion, pressureless sintering and carbo-thermal reduction is studied using XRD and electron microscopy. Electrochemical Impedance Spectroscopy measurements were performed in a three-electrode electrochemical system and showed that the oxygen vacancies in the functionally graded fibres affect the flat band potential and have increased carrier density compared to?. The efficiency of the system was evaluated with photo-electro-chemical measurements that shows higher efficiency for the functionally graded fibres compared to homogeneous TiO_2 or Magnéli phase fibres.

1. Introduction

Titania (TiO_2) has been extensively investigated as an n-type semiconductor performing as a photo-anode for photo-electro-chemical (PEC) water splitting due to its chemical resistance, environmental suitability and low cost. Another main advantage of TiO_2 is the suitable band edge positions, since a semiconductor for water splitting needs to have a minimum energy gap of 1.23eV along with conduction and valence bands overlapping the oxidation of H_2O and reduction of H^+ respectively. The main limitations of stoichiometric TiO_2 are its large band gap (3.2 eV) and high electron-hole recombination due to the short life of the excited electron. A variety of TiO_2 structures have been investigated, for example carbon-doped TiO_2 [1], hydrogen treated TiO_2 [2] and TiO_2 nanostructures [2-4] in order to achieve improved performance for water-splitting applications.

Previous work on Ti-suboxides has shown that it is possible to control the number oxygen vacancies and its electrical conductivity from 10^{-9} S/m (TiO_2) to 10^4 S/m (Magnéli phases) [5]. In this paper, we investigate the photo-electro-chemical properties of a functionally graded structure, whereby fine scale fibres are formed with a gradually increasing density of oxygen vacancies along its length. Figure 1 shows a

schematic representation of a functionally graded fibre structure with one end consisting of TiO_2 with oxygen vacancies introduced by carbo-thermal reduction and the other edge is chemically reduced to a larger extent and therefore consists primarily of Magnéli phases (Ti_nO_{2n-1}, $3<n<10$). The heavily reduced, and electrically conductive, end is then bonded with Ag wires using Al paste; which has been shown to form an ohmic electrical contact with the Magnéli phase region [5]. The photocurrent density efficiency was determined and the semiconductor-electrolyte interface was studied.

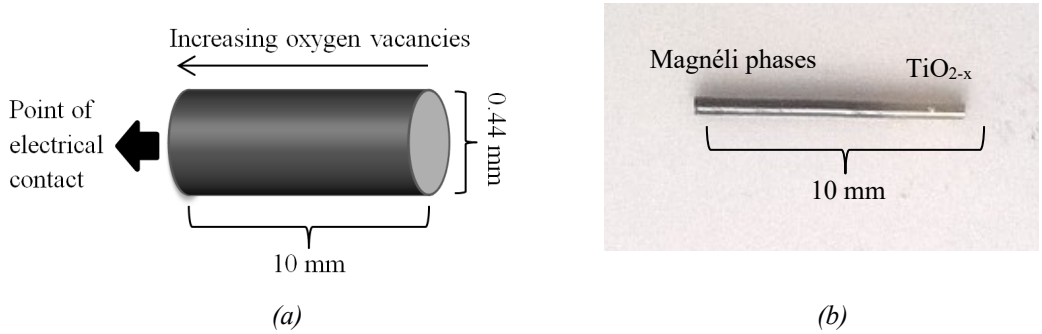

(a) *(b)*

Fig. 1: (a) Schematic representation of the composite structure of a single fibre showing the gradient oxygen vacancies across the length of the fibre and (b) image of a functionally graded fibre

2. Experimental

2.1 Materials preparation and fibre characterization

The TiO_2 fibres were produced using a thermoplastic extrusion process. Titanium dioxide powder (PI-KEM, 99.5%, 0.3 μm particle size, specific surface area 7.49 m^2/g) was pre-coated with three monolayers of stearic acid (93661, Fluka Chemie AG, Switzerland). The stearic acid was solved in toluene and mixed with the ceramic powder in a jar mill with zirconia milling media for 12h. The toluene was dried out using a rotary evaporator (Rotavapor R-134, Büchi Labortechnik AG, Switzerland). The pre-mixed powder was blended with polyethylene binder (1700MN18C Lacqtene PEBD, Arkema Group, Cedex, France) using a torque rheometer (HAAKE PolyLab Mixer, Rheomix 600, Thermo Scientific, Karlsruhe, Germany). For the two step mixing a temperature of 150°C (1st step) and 120°C (2nd step) was used. After mixing a thermoplastic homogeneous feedstock with 54 vol.% of TiO_2 powder was achieved. This feedstock was used for thermoplastic extrusion of fibres with a diameter of 500 μm using a capillary rheometer (RH7-2, Malvern, Herrenberg, Germany) at a temperature of 120°C. A special ceramic die design (Empa, Switzerland) with an orifice of 500 μm was used to produce the fibres. The fibres were extruded with a ram speed of 0.5 mm/s and a pressure of 13 MPa [6]. The 'green' TiO_2 fibres were cut on a conveyor belt into 170 mm long lengths. The 'green-body' fibres were then sintered at 1300°C for 1.5h in chamber furnace (UAF, LENTON, UK) with a dwell stage at 500°C in order to burn out the binder. This sintering pattern was selected after optimization in order to achieve high density samples (>97% of theoretical) and avoid significant grain growth. After sintering, the diameter of the stoichiometric TiO_2 fibres was 440μm.

To produce the functionally graded fibres the TiO_2 sintered fibres were reduced using a carbo-thermal process performed in a tubular furnace (LTF, LENTON, UK) with

carbon black powder as reducing agent that was in contact with one end of 10mm long fibres. The reduction process was performed at 1300°C for 1h under constant argon flow. The manufacturing and characterization of homogeneous TiO_2 and Magnéli phases fibres has been presented in detail in previous work [5]; focusing on structural and electrical characterization. In the present work these homogenous fibres (length 10 mm, ⌀ 0.44 mm) are also tested to compare with the functionally graded fibres. To characterize the structure of the graded fibres and determine the phases present at both extremes of the fibre lengths X-Ray Diffraction (XRD), Bruker D8-Advance using Cu-K alpha wavelengths, and Scanning Electron Microscopy (SEM, JEOL JSM6480LV) were used.

2.2 Characterization of photocurrents

The photocurrent of TiO_2, Magnéli phases and functional graded fibres was studied as a function of the intensity of the UV light using a novel LED reaction cell. The incident photon-to-photocurrent efficiency (IPCE) was determined according to eq. 1:

$$IPCE\ (\%) = \frac{i_{ph}.h.c}{\lambda.P.e}\ x\ 100, \qquad \text{eq.1}$$

where i_{ph} is the photocurrent density, h is Planck's constant, c velocity of light, P the light power density, λ is the irradiation wavelength, and e is the elemental charge. Photo-electro-chemical (PEC) measurements on individual fibres were performed in a three electrode electrochemical system using a saturated calomel electrode (SCE) reference electrode and a platinum wire as a counter electrode in 1M KOH electrolyte. The reaction cell was equipped with an LED board with 36 LEDs controlled in 12 individual channels of three LEDs each (Figure 2a). The arrangement of LEDs was designed to provide an even illumination within the reaction cell. The LED board is an Insulated Metal Substrate (IMS) Printed Circuit Board (PCB) for better thermal management and each LED generates 800mW of optical power at full electric power; this corresponds to ~1.9 kW/m^2 of optical power at a distance of 100mm from the LEDs. In this work, tests were conducted on single fibres using 40% of the power, i.e. at 760W/m^2. There is a ±10% variation in optical power between LEDs, as well as ±2nm variation in dominant wavelength [7]. In order to achieve an improved control of the optical power delivered to the fibres, an Electrically Erasable Programmable Read-Only Memory (EEPROM) chip was applied to the LED light source. The EEPROM holds the information about the intensity of each channel at different electrical power levels and the information on dominant wavelength offset from the desired wavelength; in this case 368 nm. Using this information the controller can adjust the input power to all channels to provide the correct optical power. Since the LEDs are heat sensitive, a temperature sensor was placed on the PCB of the UV light source and the sensor was used as an overheating protection. The LEDs were controlled with a Pulse Width Modulated (PWM) signal generated by the LED driver circuitry. These LEDs were therefore cycled between being fully on and fully off and the duty cycle of the PWM signal determines the average intensity. UV light with a wavelength of 368nm was

chosen since previous work on TiO_2 indicated that doping or oxygen vacancies have the greatest affect in this wavelength region [8-10].
The reactor used was a glass container with double walls with a space between the reactor vessel walls for a coolant to keep the temperature of the fibre in the reactor at a stable temperature (Figure 2b). Linear sweeps of potential were collected electrode using an Ivium Technologies potentiostat. The interface of the semiconductor and the electrolyte was also studied using a Solartron SI 1260 coupled with a SI 1286 dielectric interface.

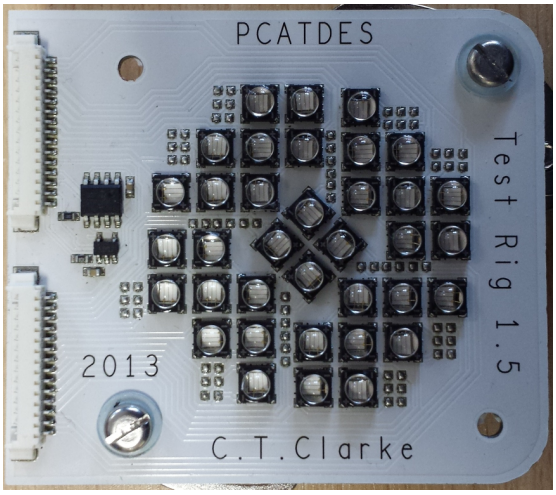

(a)

(b)

Figure 2: (a) LED array board and (b) reaction cell

For an n-type semiconductor electrode at open circuit, the Fermi level is typically higher than the redox potential of the electrolyte [11] and hence there is an upward bending of the band edges. At positive potentials the holes move towards the electrode-electrolyte interface and electrons move to the interior of the semiconductor, where the Magnéli phases are highly conductive and prevent electron-hole recombination. The gradual increase of the conductivity across the length of fibres improves the interconnectivity and the collection of the photo generated electrons at the base of the fibres [12]. At a certain potential the Fermi level is at the same energy level as the solution redox potential and therefore there is no band bending. This potential is referred to as the flat band potential (E_{fb}) which can be calculated based on the Mott-Schottky relationship by measuring the apparent capacitance as a function of the applied potential (eq. 2). The donor density can be calculated from the gradient (n) of the ($1/C^2$ vs E) curve and E_{fb} determined by extrapolation to the condition, C=0.

$$1/C^2 = 2\left(E - E_{fb} - kT/e\right) / N_D.\varepsilon.\varepsilon_0.e.A^2 \qquad \text{, eq. 2}$$

$$N_D = \frac{2}{\varepsilon\varepsilon_0.A^2.e.n} \qquad \text{, eq. 3}$$

where N_D is the carrier density, k the Boltzmann constant, T the temperature, ε the dielectric constant of the anodic film, ε_0 the permittivity of free space, e the charge of an electron and A the electrode surface. There are two capacitance values to be considered, the space charge region and the double layer. Since the space charge capacitance is much smaller than the double layer capacitance [13] the contribution of the space charge capacitance to the total capacitance is considered negligible. The equivalent circuit used for the modelling of the Electrochemical Impedance Spectroscopy measurements is an R (R-C) circuit [14].

3. Results and discussion

The morphology and structure of the functionally graded fibres were characterized by SEM and XRD. Figure 2a,b present SEM images of lightly reduced TiO_{2-x} fibre end (i.e. furthest away from carbon source) and Figure 2c,d shows the heavily reduced (Fig. 2c,d) Magnéli phase end of the functionally graded fibre.

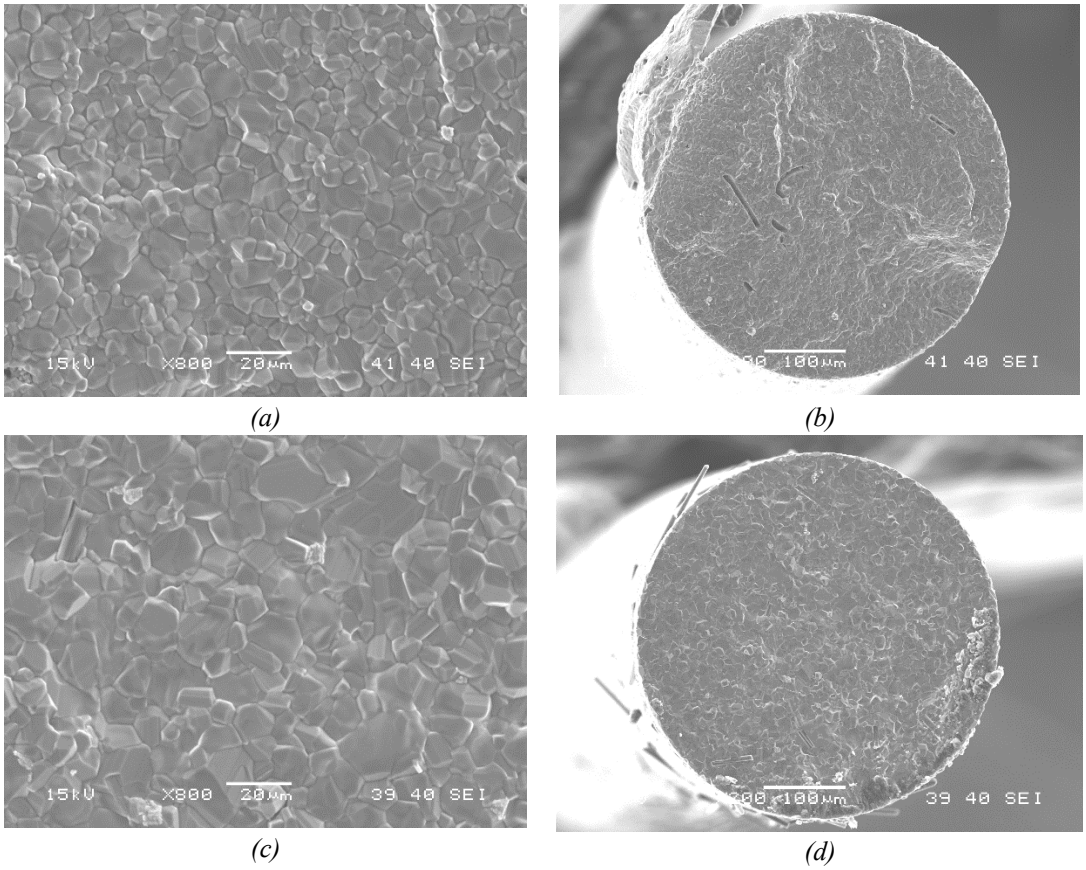

(a) *(b)* *(c)* *(d)*

Figure 2: SEM images of (a-b) the TiO_{2-x} end of functionally graded fibres and (c-d) the Magnéli phases end of the functionally fibres.

Using the linear intercept method, the measured grain size was smaller at the TiO_{2-x} end of the functionally graded fibre. The grain sizes are 5.9 and 8.3µm for the TiO_{2-x} and the Magnéli phases end respectively. At the Magnéli phase fibre end the diffusion of oxygen is more intense and this can lead to grain boundary migration that increases the grain size [15]. After sintering and reduction the diameter is 440µm across the whole

length of the fibres. XRD spectra for the functionally graded fibres are presented in figure 3 and show the different phases formed at each end of the fibres. The XRD spectrum of the TiO_{2-x} fibre end shows the presence of rutile TiO_2 and titanium suboxides while the XRD spectrum of the Magnéli phase fibre end shows only the presence of titanium suboxides and the TiO_2 peaks are no longer present.

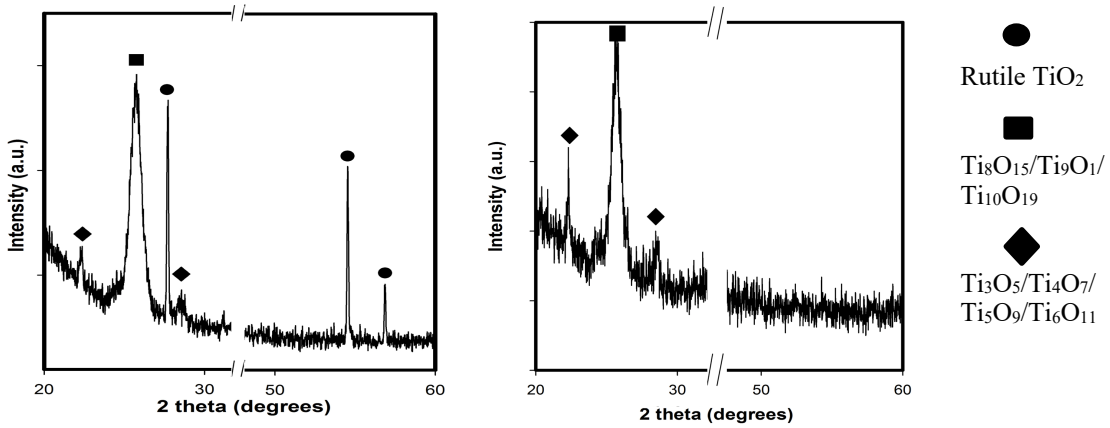

(a) *(b)*

Figure 3: XRD spectra of the opposite end of the composite fibre. (a) TiO_{2-x} end and (b) Magnéli phase end.

To investigate the effect of the oxygen vacancies on the electrode-electrolyte interface electrochemical impedance measurements on single Magnéli phases and functionally graded fibres were also conducted. Measurements conducted on single TiO_2 fibres were subject to noise due to their low electrical conductivity (10^{-9} S/m) and accurate fitting of the impedance measurements was therefore not possible. Figure 4a, b show the Mott-Schottky plots for the Magnéli phase and functionally graded fibres. Both curves exhibit positive slopes suggesting the n-type semiconductor behaviour of both materials.

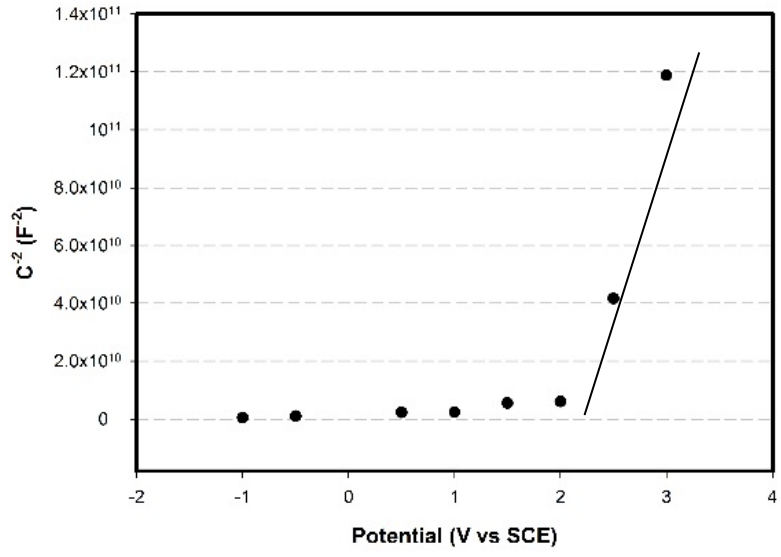

(a)

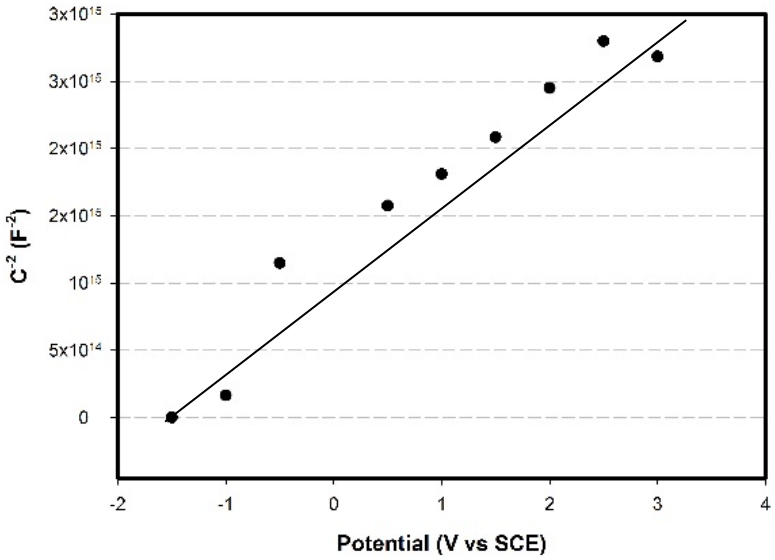

(b)

Figure 4: Mott-Schottky plots for (a) Magnéli phases single fibre and (b) functionally graded single fibre.

The flat band potential was determined to be 1.92 V vs SCE for the Magnéli phase fibre whereas for the functionally graded fibre it was -2.33 V vs SCE. The Mangéli phases exhibit 2-D electronic conductivity and therefore the number of available carries is not as high in this region compared to the TiO_{2-x} fibre end where the oxygen vacancies introduced by partial reduction increase the carrier density. By determining the gradient (*n*) of the Mott-Schottky plots in fig. 4 and using eq. 3 the carrier density was determined; for the homogenous Magnéli phase fibre the carrier density is 4.16 x 10^{14} m^{-3} and for the functionally graded fibre it has increased to 5.72 x 10^{17} m^{-3}. Oxygen vacancies are known to be shallow donors for the TiO_2 rutile phase and therefore increases the carrier density [16]. In the case of the Magnéli phases the structure and the conduction mechanism changes and thus the oxygen vacancies do not increase the carrier density [17]. The EIS measurements in Fig. 4, which show the more negative flat band potential of the functionally graded fibres, are confirmed from the photocurrent measurements shown in figure 5 which compares the photocurrent densities of TiO_2, Magnéli phase and functionally graded fibres. The photocurrent density produced from the functionally graded fibre is much higher (0.786 mA/cm^2) than both the TiO_2 (0.032 mA/cm^2) and Magnéli (0.065 mA/cm^2). The IPCE (incident photon to current conversion efficiency) was also calculated as shown in table 1 at -0.241 V vs SCE (0 V vs RHE). The TiO_2 fibre has the lowest efficiency, where the Magnéli phases fibre has an increased performance but is not as high as the functionally graded fibre, which is in agreement with the measured carrier density. In addition to the higher carrier density the functionally graded fibres have improved interconnectivity due to the gradually increasing oxygen vacancies that enhance the electron-hole separation.

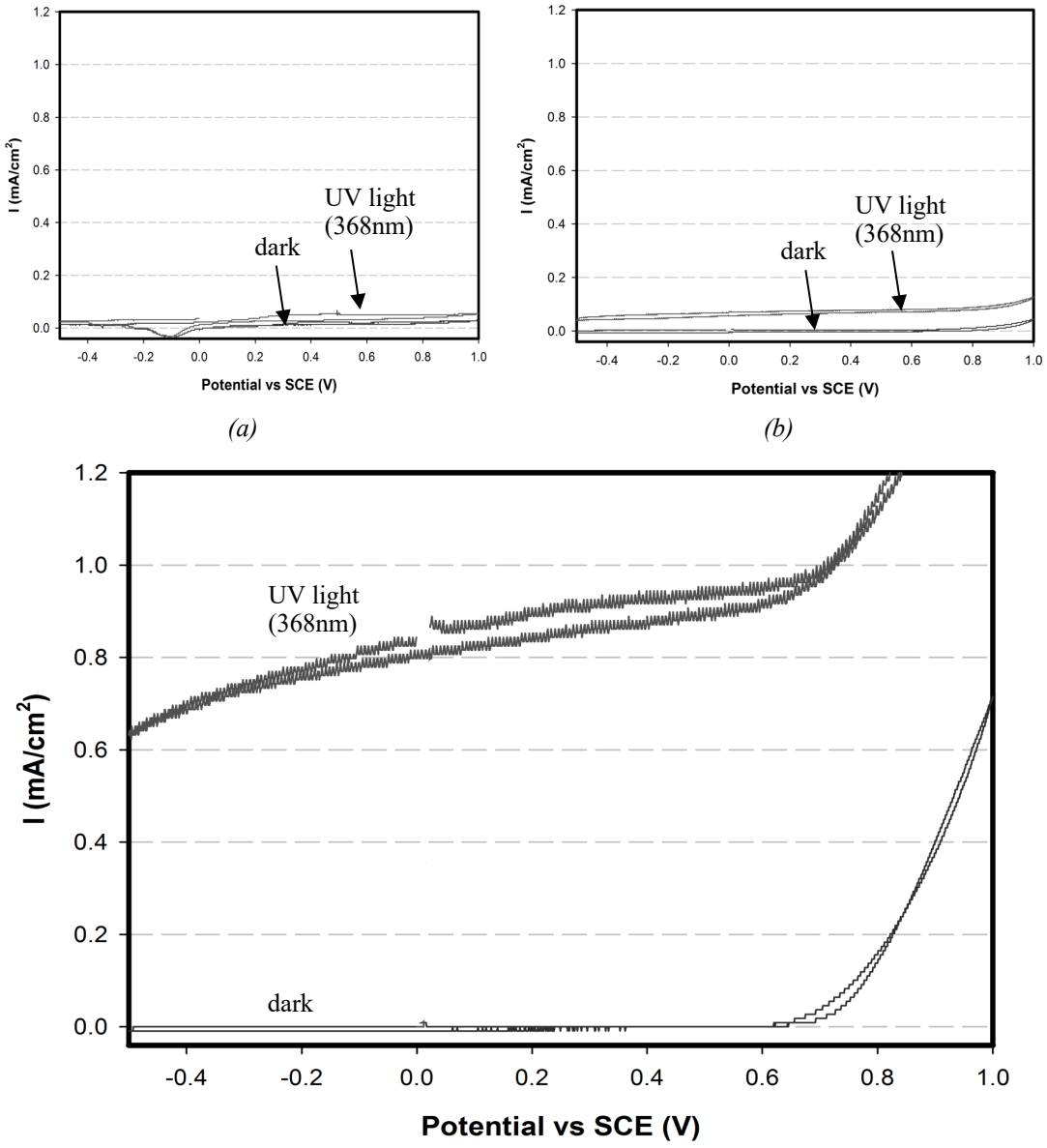

Figure 5: Photocurrent vs potential (vs SCE) under UV light of (a) TiO_2 fibre, (b) Magnéli phases fibre and (c) functionally graded fibre (760 W/m², 368nm).

Table 1: The incident photon-to-photocurrent efficiency (IPCE) of TiO_2, Magnéli phases and the functionally graded fibres (TiO_{2-x}-Magnéli phases)

Material	IPCE (%)
TiO_2	1.42
Magnéli phases	2.88
Graded (TiO_{2-x}- Magnéli phases)	34.8

The calculated IPCE for the functionally graded fibres at 368nm is higher than the efficiency reported in other work on modified TiO_2 [1, 4, 9] and therefore shows the promise of functionally graded fibres for water splitting applications. Further work on the graded fibres will include the measurement of the photocurrent under visible light, the determination of the efficiency and testing of larger scale fibre arrays.

4. Conclusions

This paper has investigated work to enhance the performance of TiO_2 as a photo anode for water splitting by forming a functionally graded and fine scale fibre that could be used as an array of active fibres. The fibres have been formed by carbo-thermal reduction on extruded TiO_2 fibres and the low-cost extrusion process is of interest to readily form large scale arrays of such structures. XRD shows that the fibre end furthest from the carbon source during the reduction process consists mostly of rutile TiO_2 along with titanium suboxides (TiO_{2-x}) due the oxygen vacancies introduced by carbo-thermal reduction. This fibre end is placed in contact with the electrolyte and acts to absorb the UV light. The fibre end that is heavily reduced and in direct contact with the carbon source during the reduction process consists of Magnéli phases that exhibit electrical conductivity close to metallic (10^4 S/m). This end of fibre is used to encourage electron-hole separation. As shown from the EIS data, the level of oxygen vacancies along the fibre length affect the flat band potential that moves to negative values (at both ends) and are therefore more beneficial for water splitting applications. In addition, the TiO_{2-x} fibre end increases the carrier density due to the increased shallow donors. The photocurrent density of the functionally graded fibres was significantly higher compared to homogeneous TiO_2 and Magnéli phases fibres reaching an efficiency of 34.8% and demonstrated the potential for functionally graded fine scale TiO_2 fibres for water splitting applications.

5. Acknowledgements

The research leading to the materials development and characterisation was from the European Union's Seventh Framework Programme (FP7/2007-2013)/ERC Grant Agreement no. 320963 on Novel Energy Materials, Engineering, Science and Integrated Systems (NEMESIS). Clarke and Sergejevs gratefully acknowledge the financial support of the European Commission under FP7 project 309846: "Photocatalytic Materials for the Destruction of Recalcitrant Organic Industrial Waste – PCATDES for reactor design.

References

1. Cheng, C., & Sun, Y. (2012). Carbon doped TiO_2 nanowire arrays with improved photoelectrochemical water splitting performance. *Applied Surface Science*, *263*, 273–276.
2. Wang, G., Wang, H., Ling, Y., Tang, Y., Yang, X., Fitzmorris, R. C., Li, Y. (2011). Hydrogen-treated TiO_2 nanowire arrays for photoelectrochemical water splitting. *Nano Letters*, *11*(7), 3026–33.
3. Regonini, D., Alves, A. K., Berutti, F. A., & Clemens, F. (2014). Effect of Aging Time and Film Thickness on the Photoelectrochemical Properties of TiO_2 Sol-Gel Photoanodes, *2014*.
4. Yu, J., Qi, L., & Jaroniec, M. (2010). Hydrogen Production by Photocatalytic Water Splitting over Pt/TiO_2 Nanosheets with Exposed (001) Facets. *The Journal of Physical Chemistry C*, *114*(30), 13118–13125.

5. Adamaki, V., Clemens, F., Ragulis, P., Pennock, S. R., Taylor, J., & Bowen, C. R. (2014). Manufacturing and characterization of Magneli phase conductive fibres. *Journal of Materials Chemistry A*, *2*(22), 8328–8333.
6. Heiber, J., Clemens, F., Graule, T., & Hülsenberg, D. (2005). Thermoplastic Extrusion to Highly-Loaded Thin Green Fibres Containing Pb(Zr,Ti)O3. *Advanced Engineering Materials*, *7*(5), 404–408.
7. http://www.ledengin.com/files/products/LZ1/LZ1-00UV00.pdf
8. Khan, S. U. M., Al-Shahry, M., & Ingler, W. B. (2002). Efficient photochemical water splitting by a chemically modified n-TiO_2. *Science (New York, N.Y.)*, *297*(5590), 2243–5.
9. Mohapatra, S. K., Misra, M., Mahajan, V. K., & Raja, K. S. (2007). Design of a Highly Efficient Photoelectrolytic Cell for Hydrogen Generation by Water Splitting: Application of $TiO_{2-x}C_x$ Nanotubes as a Photoanode and Pt/TiO_2 Nanotubes as a Cathode. *Journal of Physical Chemistry C*, *111*(24), 8677–8685.
10. Abe, R., Sayama, K., Domen, K., & Arakawa, H. (2001). A new type of water splitting system composed of two different TiO_2 photocatalysts (anatase, rutile) and a IO^{3-}/I^- shuttle redox mediator. *Chemical Physics Letters*, *344*(3-4), 339–344.
11. Lasia, A. (n.d.). Electrochemical Impedance Spectroscopy and its Applications. Retrieved January 23, 2015
12. Regonini, D., Teloeken, A. C., Alves, A. K., Berutti, F. A., Bergmann, C. P., Graule, T., & Clemens, F. (2013). Electrospun TiO_2 Fiber Composite Photoelectrodes for Water Splitting.
13. Cardon, F., & Gomes, W. P. (1978). On the determination of the flat-band potential of a semiconductor in contact with a metal or an electrolyte from the Mott-Schottky plot. *Journal of Physics D: Applied Physics*, *11*(4), L63–L67.
14. Khan, S. U. M., & Akikusa, J. (1999). Photoelectrochemical Splitting of Water at Nanocrystalline n -Fe_2O_3 Thin-Film Electrodes. *The Journal of Physical Chemistry B*, *103*(34), 7184–7189.
15. Raj, R., & Ashby, M. F. (1971). On grain boundary sliding and diffusional creep. *Metallurgical Transactions*, *2*(4), 1113–1127.
16. Janotti, A., Varley, J. B., Rinke, P., Umezawa, N., Kresse, G., & Van de Walle, C. G. (2010). Hybrid functional studies of the oxygen vacancy in TiO_2. *Physical Review B*, *81*(8), 085212.
17. Regonini, D., Adamaki, V., Bowen, C. R., Pennock, S. R., Taylor, J., & Dent, A. C. E. (2012). AC electrical properties of TiO2 and Magnéli phases, Ti_nO_{2n-1}. *Solid State Ionics*, *229*, 38–44.